ISSN: 1692-7257 - Volume 1 – Number 45 - 2025

RCTA
Revista Colombiana de Tecnologías de Avanzada
UNIPAMPLONA

Digital Object Identifier: 10.24054/rcta.v1i45.3279

Proposal of a method for asbestos detection in hyperspectral images based on spectral differential similarity

Propuesta de un método computacional para la detección de asbesto en imágenes hiperespectrales a partir de la similitud diferencial espectral

PhD. Gabriel Elías Chanchí Golondrino[1], PhD. Manuel Saba[1]
PhD. Manuel Alejandro Ospina Alarcón[1]

[1] ***Universidad de Cartagena,*** *Facultad de Ingeniería, Programa de Ingeniería de Sistemas, Cartagena de Indias, Bolívar, Colombia.*

Correspondencia: *gchanchig@unicartagena.edu.co*

Received: *july 01, 2024.* ***Accepted:*** *november 16, 2024.* ***Published:*** *january 01, 2025.*

How to cite: *G. E. Chanchí Golondrino, M. Saba, and M. A. Ospina Alarcón, "Proposal of a method for asbestos detection in hyperspectral images based on spectral differential similarity", RCTA, vol. 1, no. 45, pp. 195–203, jan. 2025. Recovered from https://ojs.unipamplona.edu.co/index.php/rcta/article/view/3279*

Abstract: Considering that one of the challenges of hyperspectral imaging is identifying methods that enable the effective and efficient detection of materials, this article proposes a new method for detecting asbestos in hyperspectral images based on spectral differential similarity. This method determines how closely the spectral signature of a given pixel matches the spectral signature of asbestos. The proposed method was implemented using open-source libraries such as spectral, numpy, pandas, and matplotlib. Compared to the correlation method, it detected 0.813% fewer vegetation pixels. In terms of computational efficiency, the proposed method was 4.27 times faster than the correlation method. The results indicate that the proposed method demonstrates adequate efficacy and excellent efficiency, making it a strong candidate for integration into tools for processing and analyzing hyperspectral images in academic and industrial domains.

Keywords: Asbestos, correlation, hyperspectral imaging, spectral signature, remote sensing.

Resumen: Teniendo en cuenta que uno de los desafíos de las imágenes hiperespectrales es la identificación de métodos que permitan la detección de materiales de manera eficaz y eficiente, en este artículo se propuso un nuevo método para la detección de asbesto en imágenes hiperespectrales basado en la similitud diferencial espectral, a través del cual es posible determinar que tan cercana es la firma espectral de un pixel determinado con respecto a la firma espectral del asbesto. El método propuesto fue implementado mediante el uso de librerías del dominio del código abierto tales como: spectral, numpy, pandas y matplotlib, obteniendo que con respecto al método de correlación fue detectado un 0.813% menos pixeles de vegetación. Así mismo, se obtuvo a nivel de la eficiencia computacional que el método propuesto resultó 4.27 veces más rápido que el método de correlación. Los resultados obtenidos permiten concluir que el método propuesto presenta una adecuada

eficacia y una excelente eficiencia, lo cual permite que pueda ser considerado para ser integrado en herramientas para el procesamiento y análisis de imágenes hiperespectrales en el dominio académico y empresarial.

Palabras clave: Asbesto, correlación, imagen hiperespectral, firma espectral, sensado remoto.

1. INTRODUCTION

Hyperspectral images (HSI) play a fundamental role in remote sensing by providing detailed spectral information that enables the identification and analysis of various types of materials through the detection of electromagnetic waves reflected by objects [1]. In this context, HSI capture data across a wide range of wavelengths, from ultraviolet to infrared, allowing for a detailed analysis of materials and their properties by combining high spectral resolution with spatial accuracy. This combination is particularly useful in applications such as precision agriculture, where detailed observation optimizes agricultural processes [2]. Hyperspectral imaging systems generate what are known as datacubes, which collect data from hundreds of narrow spectral bands for each pixel in the image [3].

Hyperspectral imaging (HSI) has been applied across various fields. In precision agriculture, HSI has been widely used for crop classification, disease detection, and monitoring of crop conditions such as maturity and nutrient status [4], [5]. Similarly, in environmental contexts, HSI is employed to categorize and identify the composition of different surface elements, such as vegetation, water, soil, and urban areas, enabling natural resource management and environmental change monitoring [4], [6]–[8]. In geology, HSI facilitates the evaluation and identification of the composition, morphology, and structure of materials, making it a key tool for exploration and monitoring in earth sciences [9]. Additionally, HSI has enabled precise mapping and identification of mineral distributions in geological samples, including carbonate rocks and drill cores, through the analysis of their spectral signatures [10]–[12]. In the military domain, HSI has been used for the detection and recognition of low-signature targets, which are challenging to identify due to their camouflage or low emissions. This provides a significant tactical advantage by allowing precise localization of discrete targets, subpixel-level target detection, distinction of concealed features and camouflages, identification of chemical agents, and detection of disturbed soil over buried objects [13]–[15]. In public health, HSI has been essential for identifying asbestos in construction and demolition waste using the short-wave infrared range (SWIR: 1000–2500 nm) and detecting asbestos in urban rooftops. This is critical as asbestos poses a serious health risk, being linked to severe respiratory diseases, making its detection and control a public health priority [16]–[18]. Moreover, hyperspectral imaging for asbestos detection offers a more efficient and cost-effective alternative compared to traditional laboratory-based identification methods [19].

In addressing the challenges in the field of HSI, it is important to highlight that the large volume of data generated due to its high dimensionality demands significant storage and processing capabilities, which often necessitates the use of dimensionality reduction techniques to manage its complexity [6], [7], [20], [21]. Although effective and widely adopted techniques, such as supervised learning methods, are available for material detection in hyperspectral images, scalable solutions like distributed cloud training are required to handle data more efficiently in this context [22]. Similarly, the high dimensionality of hyperspectral data necessitates the implementation of advanced processing techniques to effectively manage the large data volumes [23], [24]. As an alternative to the challenge of high dimensionality, various approaches have been proposed, including feature selection and information gain methods, aiming to preserve relevant information while reducing dimensionality [25], [26].

In light of the aforementioned challenges related to dimensionality and processing efficiency in hyperspectral imaging, this article introduces a novel computational method for asbestos detection in hyperspectral images. The proposed method is based on evaluating the similarity between a pixel in the hyperspectral image and the spectral signature of asbestos, using the spectral difference between normalized reflectance curves. The method was implemented using open-source libraries such as spectral, numpy, pandas, matplotlib, and scipy. The evaluation of the proposed method was conducted on a reference hyperspectral image from the Manga neighborhood in Cartagena. Its effectiveness in

detection and computational efficiency were compared to the correlation method, which has been widely reported in the literature for material detection in hyperspectral images [27], [28]. This work makes a significant contribution to the dissemination of asbestos detection methods in urban environments, as exposure to this material is linked to severe health issues such as lung cancer and mesothelioma, making its identification a public health priority [29]. By promoting and leveraging these technologies, governmental authorities can better plan and prioritize intervention strategies, optimizing resource allocation for asbestos removal [16], [30]. Furthermore, the results obtained and the consideration of dimensionality challenges in hyperspectral imaging aim to expand the range of efficient detection options in this field, ensuring that the method can be applied in both academic and industrial settings for the identification of various materials.

The remainder of the article is organized as follows: Section 2 outlines the methodological phases employed in the development of this research. Section 3 presents the results obtained in this work, including the characterization of the spectral signature of asbestos from the reference image, the determination of detection thresholds for asbestos, the implementation of the computational method, and, finally, the evaluation of the method's efficiency and effectiveness compared to the correlation method. Lastly, Section 4 provides the conclusions and future work derived from this research.

2. METHODOLOGY

The development of this research was structured into four methodological phases: P1. Selection of sample pixels and identification of the characteristic pixel, P2. Implementation and determination of the reference thresholds for the method, P3. Deployment of the method on the reference image, and P4. Comparative evaluation of the proposed method.

In Phase 1 of the methodology, a reference hyperspectral image from the Manga neighborhood in Cartagena de Indias was initially selected, with dimensions of 850 pixels in width, 725 pixels in height, and a total of 380 spectral bands. Subsequently, visual inspection sampling was conducted on the reference image, selecting 75 pixels corresponding to asbestos and 75 pixels corresponding to other materials (vegetation, water, metal roofs, roads, etc.). These pixels will later be used to determine the reference thresholds for asbestos detection using the proposed method.

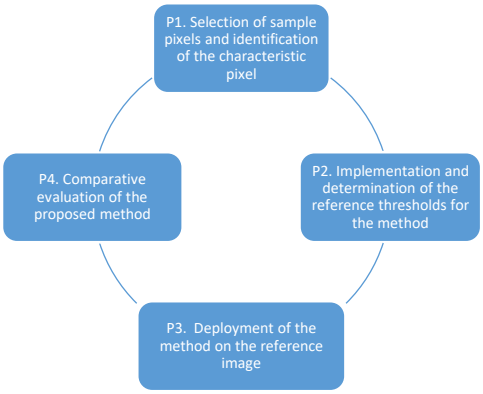

***Fig. 1**. Methodology considered for the development of the research.*
***Source:** Own elaboration.*

The above is illustrated in Fig. 2, where the selected asbestos pixels are shown in blue, and the pixels corresponding to other materials are shown in red.

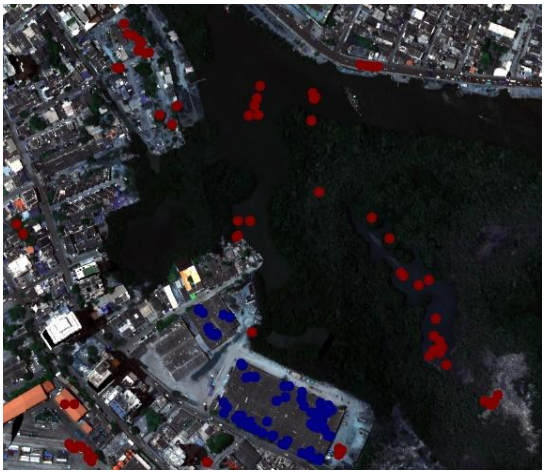

***Fig. 2**. Selected sample pixels.*
***Source:** Own elaboration.*

From the selected asbestos pixels, the average pixel was calculated, capturing the mean normalized reflectance of the asbestos pixels across its 380 bands (see Fig. 3). This pixel is highly useful as it will be used to operate and correlate with various types of pixels to determine how similar the pixels in the image are to the characteristic asbestos pixel.

In Phase 2 of the methodology, the spectral differential similarity method was implemented using the advantages provided by Python's numpy library. This method was developed based on Equation (1), which calculates the percentage similarity between two pixels by subtracting the characteristic pixel from a given pixel in the image.

$$sim\_perc = 100 - \frac{\sum_{i=1}^{n}\lceil pix_i - avg\_pix\rceil}{n} x100 \quad (1)$$

In Equation (1), $\sum_{i=1}^{n}\lceil pix_i - \text{avg\_pix}\rceil$ represents the summation of absolute differences between a given pixel i and the characteristic or average pixel at the level of the n bands that make up the hyperspectral image, where n = 380 in this case. Thus, the closer a pixel is to the average pixel, the summation approaches 0, and the percentage similarity tends toward 0. Similarly, since the image has normalized reflectance values, the worst-case difference between bands will be 1, resulting in a total summation of 380, where the similarity will approach 100. Once the proposed method was implemented using Python libraries, its effectiveness was evaluated using the 75 asbestos pixels and the 75 non-asbestos pixels. In both cases, the minimum and maximum similarity percentages were determined using Equation (1). Based on this, a detection threshold was established as the minimum similarity percentage for asbestos pixels, ensuring that this value does not overlap with the maximum similarity percentage obtained for non-asbestos pixels.

In Phase 3 of the methodology, the method was applied to all pixels in the image using the threshold determined in Phase 2, coloring the pixels where the presence of asbestos was detected. It is worth mentioning that each detected asbestos pixel was counted to determine the percentage of asbestos pixels present in the reference image. Additionally, the similarity operations were performed on the normalized representation of the image, as Equation (1) is designed to operate on normalized reflectance values. The percentage of asbestos pixels identified in the reference image was then compared to the percentage obtained using the correlation method to evaluate the effectiveness of the proposed method.

Finally, in Phase 4 of the methodology, the efficiency of the spectral difference method was compared with the correlation method by executing both on a square region of the image measuring 50x50x380 pixels a predetermined number of times (20, 40, 60, 80, and 100 repetitions). The objective was to calculate the average execution time for each method and determine which demonstrates greater computational efficiency.

3. RESULTS

Once the 75 sample pixels of asbestos and the 75 pixels of other materials were selected, as described in the methodology, the first step was to obtain the characteristic pixel or spectral signature of the 75 asbestos pixels. This was achieved by averaging the normalized reflectance values across the 380 bands, resulting in the characteristic spectral signature of asbestos, which is presented in Fig. 3.

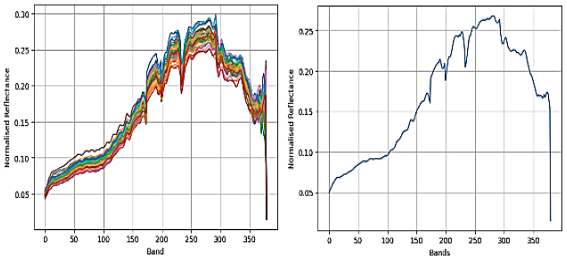

Fig. 3. *Characteristic pixel obtained for asbestos.* ***Source:*** *Own elaboration.*

Based on the characteristic pixel obtained, the spectral differential similarity method was implemented in Python and evaluated using the sample pixels of asbestos and other materials. In Fig. 4, the implementation of the mentioned method is shown from left to right, first with the 75 sample asbestos pixels and then with the non-asbestos pixels, aiming to determine the thresholds that can be used for asbestos detection in the complete reference hyperspectral image.

```
l_porc_diff=[]
for pix in l_pix_asb:
  diff=np.abs(pix-pix_prom)
  porc=100-(np.sum(diff)/380)*100
  l_porc_diff.append(porc)
arr_porc_diff=np.asarray(l_porc_diff)
print("Avg:",arr_porc_diff.mean())
print("Max:",arr_porc_diff.max())
print("Min: ",arr_porc_diff.min())
```

```
Avg: 99.3049054354952
Max: 99.8380234366969
Min:  97.25883508983411
```

```
l_porc_diff=[]
for pix in l_pix_no_asb:
  diff=np.abs(pix-pix_prom)
  porc=100-(np.sum(diff)/380)*100
  l_porc_diff.append(porc)
arr_porc_diff=np.asarray(l_porc_diff)
print("Avg:",arr_porc_diff.mean())
print("Max:",arr_porc_diff.max())
print("Min:",arr_porc_diff.min())
```

```
Avg: 91.12311636570678
Max: 96.77609293084396
Min: 86.39467138993112
```

Fig. 4. *Evaluation of the method with asbestos and non-asbestos pixels.* ***Source:*** *Own elaboration.*

From the execution of the scripts shown in Fig. 4, the minimum, maximum, and average spectral differential similarity percentages were obtained, as presented in Fig. 5. It can be observed that there is no overlap between the minimum spectral differential similarity percentage for asbestos pixels (97.259%) and the maximum spectral differential similarity percentage for non-asbestos pixels (96.776%), with a percentage difference of 0.483% between these two values. Thus, the minimum detection threshold for asbestos pixels that can be considered for the complete image is 97.259%.

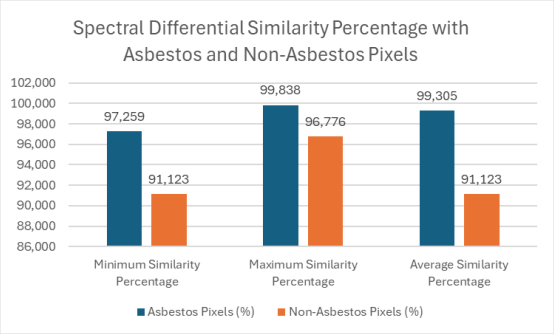

***Fig. 5**. Spectral difference percentages obtained with asbestos and non-asbestos pixels.*
***Source:** Own elaboration.*

Similarly, it is worth mentioning that when implementing the correlation method on the same 75 sample pixels of asbestos and other materials, the results presented in Fig. 6 were obtained.

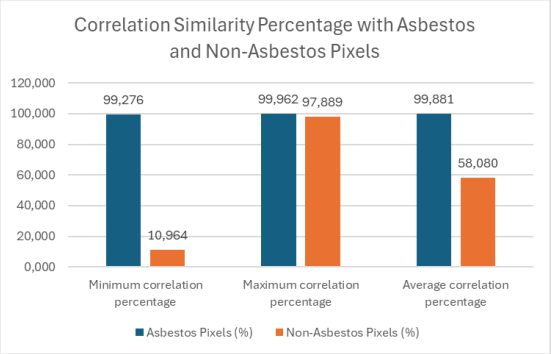

***Fig. 6**. Correlation percentages obtained with asbestos and non-asbestos pixels.*
***Source:** Own elaboration.*

From Fig. 6, it can be observed that in the case of the correlation method, the difference in similarity between the minimum correlation percentage for asbestos pixels and the maximum correlation percentage for non-asbestos pixels is 1.387%. This difference is 2.87 times greater than the difference obtained using the spectral differential similarity method (0.483%). Despite this, in both cases, the methods show no overlap in the identification of asbestos and non-asbestos pixels, and the spectral differential similarity method can be effectively used for detecting this material.

Once the thresholds for the spectral differential similarity method were identified, both this method and the correlation method were applied to the complete reference image to evaluate their effectiveness in detecting the percentage of the image corresponding to asbestos. The results of these methods applied to the reference image are presented in Fig. 7, where the detected asbestos pixels are shown in blue for both methods. It is important to note that both methods utilize the spectral signature or average asbestos pixel to operate with the remaining pixels in the image.

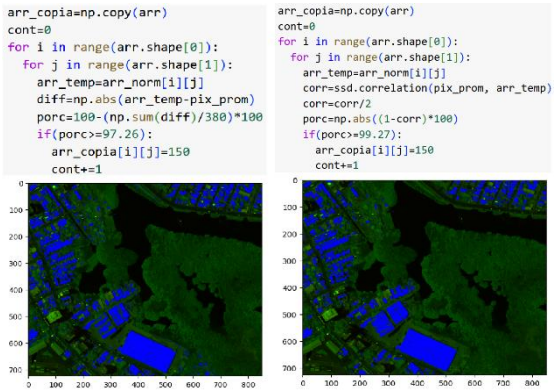

```
arr_copia=np.copy(arr)
cont=0
for i in range(arr.shape[0]):
  for j in range(arr.shape[1]):
    arr_temp=arr_norm[i][j]
    diff=np.abs(arr_temp-pix_prom)
    porc=100-(np.sum(diff)/380)*100
    if(porc>=97.26):
      arr_copia[i][j]=150
      cont+=1
```

```
arr_copia=np.copy(arr)
cont=0
for i in range(arr.shape[0]):
  for j in range(arr.shape[1]):
    arr_temp=arr_norm[i][j]
    corr=ssd.correlation(pix_prom, arr_temp)
    corr=corr/2
    porc=np.abs((1-corr)*100)
    if(porc>=99.27):
      arr_copia[i][j]=150
      cont+=1
```

***Fig. 7**. Detection of asbestos on the reference hyperspectral image using the spectral similarity and correlation methods.*
***Source:** Own elaboration.*

From the full-image scan performed by the two implemented methods, the percentage of the image containing asbestos pixels was determined based on the pixel count conducted by both methods, as shown in Fig. 8. Specifically, as illustrated in Fig. 8, the spectral differential similarity method identified 10.623% of the pixels as asbestos, while the correlation method identified 9.81%, resulting in a percentage difference of 0.813%.

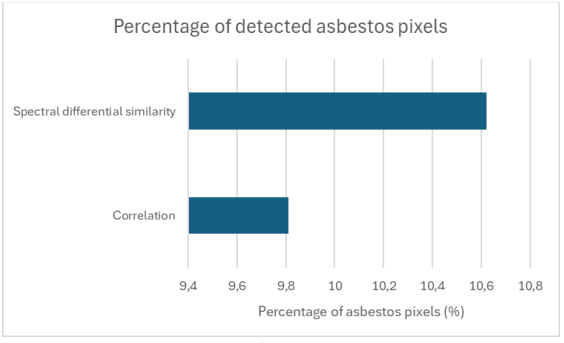

***Fig. 8**. Percentage of asbestos pixels detected.*
***Source:** Own elaboration.*

The aforementioned results can be explained by the fact that the correlation method exhibits a larger difference between the minimum percentage value for asbestos pixels and the maximum percentage value for non-asbestos pixels. This results in a lower tendency to misclassify asbestos pixels as other types of pixels. However, both methods yield very similar percentage values for detected asbestos, indicating that the spectral differential similarity method can be considered suitable for detecting asbestos in hyperspectral images due to its low margin of error compared to the correlation method.

Once the effectiveness of the spectral differential similarity method was compared to the correlation method, the computational efficiency of these two methods was also evaluated. For this purpose, a region of 100x100 pixels, each with 380 bands, was selected. Both methods were executed 20, 40, 60, 80, and 100 times on this region to calculate the average time taken by each method to process the selected region and determine the efficiency of one method relative to the other. A portion of the reference image was used to conduct these executions, as performing multiple runs on the full image would require considerable time and resources. The results of the average execution time for the two methods across the different repetitions are presented in Table 1.

Table 1: *Average execution time per repetitions*

Repetitions	Average execution time – correlation (s)	Average execution time – spectral differential similarity (s)
20	0.542	0.124
40	0.562	0.114
60	0.543	0.136
80	0.540	0.137
100	0.537	0.127
Avg	0.545	0.128

Source: *Own elaboration.*

According to the results presented in Table 1, it can be observed that for the different groups of repetitions, the correlation method has an average execution time of approximately 0.545 seconds, while the spectral differential similarity method has an average execution time of approximately 0.128 seconds. This indicates that the spectral differential similarity method is 4.27 times faster than the correlation method. This finding is further illustrated in the graph presented in Fig. 9, which shows that for the various executions, the time required by the correlation method is four times greater.

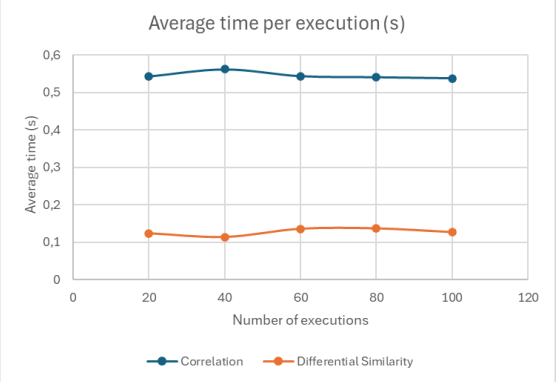

Fig. 9*. Average time per execution in the two methods.*
Source: *Own elaboration.*

Based on the above, it can be concluded that the spectral differential similarity method demonstrates significantly greater efficiency compared to the correlation method, a crucial advantage given the large dimensions of hyperspectral datacubes generated in urban area analyses. This method not only maintains comparable effectiveness to the correlation method but is also 4.27 times faster, making it an ideal alternative for integration into hyperspectral image analysis systems. Its combination of high precision and speed optimizes analysis processes, enabling more agile and effective management of the large volumes of data required for these studies.

3. CONCLUSIONS AND FUTURE WORK

Considering that one of the key challenges in hyperspectral image processing is the identification of methods capable of efficiently processing the datacube representing the image while effectively detecting materials, this article introduces a novel method for identifying the spectral differential similarity between asbestos pixels and other materials. This method aims to serve as an alternative for inclusion in studies and tools for hyperspectral image analysis in academic or industrial contexts, given the results obtained in terms of both effectiveness and efficiency.

When comparing the effectiveness of the spectral differential similarity method to the correlation method, it is observed that the proposed method achieved a similar percentage of identified asbestos pixels, with a difference of 0.81% in the proportion of pixels detected. This result considers that the difference between the minimum similarity percentage for asbestos pixels and the maximum similarity percentage for non-asbestos pixels (0.483%) is smaller than the difference obtained with the correlation method (1.387%). Thus, although the correlation method has a slightly higher detection threshold, the difference in detected pixels is less than 1%, indicating that the effectiveness of the proposed method can be considered adequate.

When comparing the computational efficiency of the proposed method to the correlation-based method, it was concluded that the spectral differential similarity method is 4.27 times faster across the various repetitions performed on a region of the reference hyperspectral image. This improvement represents a significant advantage, particularly in the analysis of urban hyperspectral images, where datacubes often have considerable

dimensions. The ability to drastically reduce processing times not only optimizes analysis in high-demand computational environments but also enables the tackling of more complex problems in less time, fostering more efficient and scalable applications in fields such as remote sensing, urban planning, and environmental management.

This study demonstrated that open-source tools and libraries are an effective alternative to proprietary tools for the detection of materials in hyperspectral images, given the high costs associated with such tools for the academic community. In this regard, the spectral library proved highly useful for extracting spectral band data from the image used in this research. Similarly, the numpy library was essential for implementing the spectral differential similarity method and calculating the average pixel. Additionally, the pandas library was instrumental in loading the data points corresponding to the sample pixels of asbestos and non-asbestos. Finally, the matplotlib library facilitated the generation of graphs for asbestos pixels, non-asbestos pixels, and the characteristic pixel.

As future work derived from this research, the aim is to improve the effectiveness of asbestos pixel detection, for instance, by using techniques to penalize out-of-range differences. This approach could enhance the difference between the minimum similarity percentage for asbestos pixels and the maximum similarity percentage for non-asbestos pixels. Similarly, comparisons of efficiency will be conducted between the proposed method and machine learning methods that have proven effective in detecting materials in hyperspectral images.

ACKNOWLEDGEMENT

The authors of this article extend their gratitude to the University of Cartagena for the support provided during the development of this research.

REFERENCES

[1] X. Zhang, “Hyperspectral image classification based on convolutional neural network,” Appl. Comput. Eng., vol. 42, no. 1, pp. 239–242, Feb. 2024, doi: 10.54254/2755-2721/42/20230783.

[2] V. K. Munipalle, U. R. Nelakuditi, M. K. C. V. S. S. , and R. R. Nidamanuri, “Ultra-high-resolution hyperspectral imagery datasets for precision agriculture applications,” Data Br., vol. 55, p. 110649, Aug. 2024, doi: 10.1016/j.dib.2024.110649.

[3] Érica S. Pinto, Gustavo Pessin, and Alan K. Rêgo Segundo, “Análise de Imagens Hiperespectrais para reconhecimento de depósitos de minério de ferro utilizando aprendizado não supervisionado,” Oct. 2022. doi: 10.20906/CBA2022/3462.

[4] Alanazi, N. H. A. Wahab, and B. A. S. Al-Rimy, “Hyperspectral Imaging for Remote Sensing and Agriculture: A Comparative Study of Transformer-based Models,” in 2024 IEEE 14th Symposium on Computer Applications & Industrial Electronics (ISCAIE), May 2024, pp. 129–136. doi: 10.1109/ISCAIE61308.2024.10576233.

[5] Y. E. García-Vera, A. Polochè-Arango, C. A. Mendivelso-Fajardo, and F. J. Gutiérrez-Bernal, “Hyperspectral Image Analysis and Machine Learning Techniques for Crop Disease Detection and Identification: A Review,” Sustainability, vol. 16, no. 14, p. 6064, Jul. 2024, doi: 10.3390/su16146064.

[6] C. Vairavan, B. M. Kamble, A. G. Durgude, S. R. Ingle, and K. Pugazenthi, “Hyperspectral Imaging of Soil and Crop: A Review,” J. Exp. Agric. Int., vol. 46, no. 1, pp. 48–61, Jan. 2024, doi: 10.9734/jeai/2024/v46i12290.

[7] C. Harsha Vardhan, R. S. Vaddi, J. Kadavakollu, and K. Kalpana, “Classification of Hyperspectral Remote Sensing Images Using Deep Learning,” 2024, pp. 349–358. doi: 10.1007/978-981-99-6547-2_27.

[8] S. Qian, “Overview of Hyperspectral Imaging Remote Sensing from Satellites,” in Advances in Hyperspectral Image Processing Techniques, Wiley, 2022, pp. 41–66. doi: 10.1002/9781119687788.ch2.

[9] M. Akewar and M. Chandak, “Hyperspectral Imaging Algorithms and Applications: A Review.” Jan. 02, 2024. doi: 10.36227/techrxiv.24743562.v2.

[10] R. J. Murphy, M. J. Van Kranendonk, S. J. Kelloway, and I. E. Wainwright, “Complex patterns in fossilized stromatolites revealed by hyperspectral imaging (400–2496 nm),” Geobiology, vol. 14, no. 5, pp. 419–439, Sep. 2016, doi: 10.1111/gbi.12184.

[11] N. Zaini, F. Van der Meer, and H. Van der Werff, “Determination of Carbonate Rock Chemistry Using Laboratory-Based Hyperspectral Imagery,” Remote Sens., vol. 6, no. 5, pp. 4149–4172, May 2014, doi: 10.3390/rs6054149.

[12] E. A. MacLagan, E. L. Walton, C. D. K. Herd, and B. Rivard, “Hyperspectral imaging of drill

core from the Steen River impact structure, Canada: Implications for hydrothermal activity and formation of suevite-like breccias," Meteorit. Planet. Sci., vol. 55, no. 7, pp. 1564–1580, Jul. 2020, doi: 10.1111/maps.13388.

[13] D. Manolakis, E. Truslow, M. Pieper, T. Cooley, and M. Brueggeman, "Detection Algorithms in Hyperspectral Imaging Systems: An Overview of Practical Algorithms," IEEE Signal Process. Mag., vol. 31, no. 1, pp. 24–33, Jan. 2014, doi: 10.1109/MSP.2013.2278915.

[14] M. Shimoni, R. Haelterman, and C. Perneel, "Hypersectral Imaging for Military and Security Applications: Combining Myriad Processing and Sensing Techniques," IEEE Geosci. Remote Sens. Mag., vol. 7, no. 2, pp. 101–117, Jun. 2019, doi: 10.1109/MGRS.2019.2902525.

[15] X. Briottet et al., "Military applications of hyperspectral imagery," in Defense and Security Symposium, May 2006, p. 62390B. doi: 10.1117/12.672030.

[16] E. Viero, D. Gubiani, M. Basso, M. Marin, and G. Sgrazzutti, "Identification of asbestos roofing from hyperspectral images." Mar. 09, 2024. doi: 10.5194/egusphere-egu24-15565.

[17] G. Bonifazi, G. Capobianco, S. Serranti, S. Malinconico, and F. Paglietti, "ASBESTOS DETECTION IN CONSTRUCTION AND DEMOLITION WASTE ADOPTING DIFFERENT CLASSIFICATION APPROACHES BASED ON SHORT WAVE INFRARED HYPERSPECTRAL IMAGING," Detritus, no. 20, pp. 90–99, Aug. 2022, doi: 10.31025/2611-4135/2022.15211.

[18] G. Bonifazi et al., "Asbestos detection in construction and demolition waste by different classification methods applied to short-wave infrared hyperspectral images," Spectrochim. Acta Part A Mol. Biomol. Spectrosc., vol. 307, p. 123672, Feb. 2024, doi: 10.1016/j.saa.2023.123672.

[19] D. Enrique Valdelamar Martínez, M. Saba, and L. K. Torres Gil, "Assessment of asbestos-cement roof distribution and prioritized intervention approaches through hyperspectral imaging," Heliyon, vol. 10, no. 3, p. e25612, Feb. 2024, doi: 10.1016/j.heliyon.2024.e25612.

[20] D. D. Langer, T. A. Johansen, and A. J. Sorensen, "Interactive Hyperspectral Data Inspection During Field Operations," in 2022 12th Workshop on Hyperspectral Imaging and Signal Processing: Evolution in Remote Sensing (WHISPERS), Sep. 2022, pp. 1–5. doi: 10.1109/WHISPERS56178.2022.9955108.

[21] V. K. Munipalle, U. Rani Nelakuditi, and R. R. Nidamanuri, "Impact of Dimensionality Reduction Techniques on Classification of Hyperspectral Images," in 2023 3rd International Conference on Intelligent Technologies (CONIT), Jun. 2023, pp. 1–6. doi: 10.1109/CONIT59222.2023.10205828.

[22] J. M. Haut, J. M. Franco-Valiente, M. E. Paoletti, S. Moreno-Álvarez, and A. Pardo-Diaz, "Hyperspectral Image Analysis Using Cloud-Based Support Vector Machines," SN Comput. Sci., vol. 5, no. 6, p. 719, Jul. 2024, doi: 10.1007/s42979-024-03073-z.

[23] S. Li, W. Song, L. Fang, Y. Chen, P. Ghamisi, and J. A. Benediktsson, "Deep Learning for Hyperspectral Image Classification: An Overview," IEEE Trans. Geosci. Remote Sens., vol. 57, no. 9, pp. 6690–6709, Sep. 2019, doi: 10.1109/TGRS.2019.2907932.

[24] Plaza et al., "Recent advances in techniques for hyperspectral image processing," Remote Sens. Environ., vol. 113, pp. S110–S122, Sep. 2009, doi: 10.1016/j.rse.2007.07.028.

[25] K. Saheb Ettabaa and M. Ben Salem, "Adaptive Progressive Band Selection for Dimensionality Reduction in Hyperspectral Images," J. Indian Soc. Remote Sens., vol. 46, no. 2, pp. 157–167, Feb. 2018, doi: 10.1007/s12524-017-0691-9.

[26] Elmaizi, H. Nhaila, E. Sarhrouni, A. Hammouch, and C. Nacir, "A novel information gain based approach for classification and dimensionality reduction of hyperspectral images," Procedia Comput. Sci., vol. 148, pp. 126–134, 2019, doi: 10.1016/j.procs.2019.01.016.

[27] G. E. Chanchí Golondrino, M. A. Ospina Alarcón, and M. Saba, "Vegetation Identification in Hyperspectral Images Using Distance/Correlation Metrics," Atmosphere (Basel)., vol. 14, no. 7, p. 1148, Jul. 2023, doi: 10.3390/atmos14071148.

[28] Z. Chao, F. Xianchuang, W. Tong, Z. Yuanzhi, and C. Shengbo, "Detection of Ore-Forming Elements Migrated From Rock and Soil to Vegetation Leaves Using Hyperspectral Data," Radio Sci., vol. 58, no. 8, Aug. 2023, doi: 10.1029/2022RS007580.

[29] N. OWADA, M. TOBITA, B. SINAICE, H. TORIYA, S. UTSUKI, and Y. KAWAMURA, "Development of Asbestos Containing Serpentinite Identification Method Using Hyperspectral Imaging," Int. J. Soc. Mater.

Eng. Resour., vol. 25, no. 2, pp. 189–194, Oct. 2022, doi: 10.5188/ijsmer.25.189.

[30] Y. Jeong, J. Yu, L. Wang, and H.-C. Kim, “Spatial Assessment of Asbestos Mine Remediation Effect Using Airborne Hyperspectral Imaging System.” May 15, 2023. doi: 10.5194/egusphere-egu23-1693.